Highly Uniform, Straightforward, Controllable Fabrication of Copper Nano-Objects via Artificial Nucleation-Assisted Electrodeposition

Joonwon Lim, Ki-Hwan Kim, Costel Sorin Cojocaru

Journal of Electroanalytical Chemistry (2021) 115594

Highly Uniform, Straightforward, Controllable Fabrication of Copper Nano-Objects *via* Artificial Nucleation-Assisted Electrodeposition

Joonwon Lim[a,b,*], Ki-Hwan Kim[b], Costel-Sorin Cojocaru[b]

DOI: https://doi.org/10.1016/j.jelechem.2021.115594

[a]*Department of Information Display, Kyung Hee University, Dongdaemun-gu, Seoul, 02447, Republic of Korea*

[b]*Laboratoire de Physique des Interfaces et des Couches Minces (LPICM), CNRS UMR 7647, Ecole polytechnique, 91128 Palaiseau, France*

**Corresponding author*

Abstract

Electrochemical synthetic route to sophisticated nano-objects has been considered as a promising and reliable strategy for diverse purpose in a wide range of applications. Especially, electrodeposition using nanoporous templates has attracted intensive research interests due to the potential for realizing diverse nanostructures and delicate composition control of the resulting fabricated materials. Unfortunately, the electrochemically filling of nanomaterials into nanoporous templates are still suffering from unexpected non-uniform formation of nano-objects, originating from random nucleation in each nanopore and overgrowth from only a few nanopores. Here, we present a highly uniform, straightforward and controllable fabrication of Cu nano-objects *via* artificial nucleation-assisted electrodeposition principle using nanoporous AAO templates. Pre-electrodeposited Ni nanoparticles at the bottom of the nanopores of AAO successfully plays a role as a nucleus at the early stage of Cu electrodeposition process. The artificial nuclei enable highly uniform and stable Cu electrodeposition inside the nanopores of AAO templates by effectively suppressing the random overgrowth of Cu. Taking advantage of the stable electrodepositing behavior, we demonstrate precise control of the geometry of Cu nano-objects, uniformly dispersed over whole surfaces of substrates.

Keywords: electrodeposition, nucleation, nanomaterials, anodic aluminum oxides

1. Introduction

The rising need for advanced electrochemical technologies has continued to increase along with the ever-increasing demands for future electrochemical applications including high performance electrochemical energy conversion/storage devices and synthesis of well-ordered nanomaterial arrays for optical/sensing devices [1-5]. Electrodeposition is basically a useful and expandable electrochemical synthetic route due to its controllability, scalability, expandability and simplicity, enabling facile and diverse shape control, such as well-ordered nano-objects, uniform thin films and micro-thick foils [6-8]. For instance, thin copper (Cu) foils, widely used as a current collector for secondary lithium ion batteries, are fabricated by continuous reduction of copper ions using electrodeposition technique [9, 10]. As a representative for the synthesis of nano-sized materials using electrodeposition methods, highly ordered metal nanowires or nanoparticles have been demonstrated with various templates [11-13]. However, the versatile electrodeposition technique requires well-optimized process condition for proper final production of desired electrodeposited materials. It originates from multiple influencing process parameters, including the identity of electrolyte containing ions to be electrodeposited, the concentration of the electrolyte, the level of applied potential/current, a temperature, and a complex interplay those process parameters.

Anodic aluminum oxide (AAO) has been widely used as a nanoporous template for electrodeposition towards various nano-objects and novel nano-devices [14-20]. The controllable nanostructures of AAO templates, including shape, size and height of nanopores, facilitate customizing electrodeposition of reactants inside nanopores [21-23]. Unlike conventional electrodeposition on the typical conductive surface, electrodeposition inside nanopores requires a delicate control in the equilibrium of the concentration of reactants in the

electrolyte filled in the nano-sized pore volume for proper fabrication of nano-objects [24]. Moreover, the uniform nucleation and growth of nano-objects over all nanopores of AAO templates during the electrodeposition process is significantly important for preventing from the undesired random overgrowth of nano-objects, achieving expected nanostructures [25, 26]. Once a non-uniform electrodeposition is triggered at the early stage of an electrodeposition process at the bottom of the nanopores, the fatal overgrowth of target materials is rapidly accelerated. It eventually leads to a planar deposition on the top surface of AAO nanoporous templates, rather than stable build-up of nano-objects from the bottom of nanopores of AAO. Unfortunately, the electrodeposition technique with nanoporous templates are still suffering from such a non-uniform electrodeposition behavior among each nanopores or requiring complicated post process consisting of totally removal of the electrically resistive oxide barrier layer at the bottom of each pore and subsequent formation of metallic thin film on the opened bottom for electrical contact for electrodeposition by a vacuum-deposition or others [27-29].

Here, we present a straightforward artificial nucleation-assisted electrodeposition principle enabling highly uniform Cu nano-objects using as-prepared AAO nanoporous templates. The pre-electrodeposited nickel (Ni) nanoparticles at the bottom of the AAO template serves as an artificial nucleation for highly uniform and controllable Cu electrodeposition inside nanopores. The artificial nucleation principle leads to stable growth stage of Cu nano-objects, effectively prevents from the deadly random overgrowth of Cu on the top surface of nanoporous templates. Ni nanoparticles plays an important role as a nucleus, giving rise to a subsequent uniform and controllable Cu electrodeposition, as revealed in the investigation of the change of current value with process time (I-t curve) during electrodeposition process. Along with the novel electrodeposition principle, the precise control of the geometry of Cu nano-objects is

demonstrated over whole surfaces of substrates.

2. Experimental

2.1. Synthesis of AAO nanoporous templates

Nanoporous AAO templates were fabricated by anodizing 3 μm thick aluminum (Al) thin film. The Al thin film was sputtered on a 500 nm thick SiO_2 layer grown on Si wafer and subsequently annealed at 450 ^oC for 2 h under flowing N_2. During anodizing the Al film, the electrolytes were heavily agitated by a stir-bar, which was positioned above the sample surface. The anodization process was carried out in 0.3 M oxalic acid or 0.3 M sulfuric acid by controlling the anodization voltage with a programmable power supply (Itech Electronic IT6834). The temperature of the electrochemical baths was precisely maintained at 25 ^oC and 5 ^oC for oxalic acid and sulfuric acid, respectively. For the preparation of the 1.5 μm thick nanoporous AAO templates on conductive underlying Al thin film, the anodization time was controlled to 500 s at the optimized constant voltage according to the type of the used electrolyte. At the end of the constant voltage step, a precisely controlled voltage decrease was applied to the samples. The final value of the anodization voltage was fixed at 5.0 V, which corresponds to a final oxide barrier layer thickness of about 6 nm. Then, the AAO samples were etched in 3 wt% H_3PO_4 for 25 min at 30 ^oC.

2.2 Fabrication of Ni nanoparticles and Cu nano-objects by electrodeposition with AAO templates

Ni was electrodeposited with a pulse voltage of 5 % duty cycle consisting of 5 ms for working regime (-5.5 V vs. Ag/AgCl) and 95 ms of resting regime (0 V vs. Ag/AgCl), using the Watts

bath as electrolyte (a mixture of 330g l^{-1} $NiSO_4$, 45g l^{-1} $NiCl_2 \cdot 6H_2O$, 38g l^{-1} H_3BO_3). The electrodeposition voltage was controlled in the potentiostatic mode using a HEKRA PG310 voltage supply. Subsequent Cu electrodeposition was carried out with identical duty cycle consisting of 5 ms for working regime (-8.5 V vs. Ag/AgCl) and 95 ms of resting regime (0 V vs. Ag/AgCl) at various negative voltages, using the Cu^{2+} solution as electrolyte (a mixture of 250 g l^{-1} $CuSO_4 \cdot 5H_2O$ and 45 g l^{-1} H_3BO_3). We used the HEKRA PG310 in the three-electrode configuration with an Ag/AgCl reference electrode and a graphite as the counter electrode. POTPULSE program created by HEKRA was used as the driving program.

2.3. Characterizations

The surface morphology of synthesized materials was characterized by a field-emission scanning electron microscope (SEM) Hitachi S-4800 (Hitachi).

3. Results and discussions

3.1. Synthetic procedure of highly uniform dispersive Cu nano-objects arrays

Figure 1 represent schematic diagram of the artificial nucleation-assisted electrodeposition process. 3 μm-thick Al thin films prepared by sputtering on SiO_2/Si substrates were anodized in 0.3 M oxalic acid at initial and final voltages of 40 V and 5V, using exponential voltage decreasing technique to obtain thin barrier oxide layer at the bottom of anodized Al thin films (Figure S1) [24]. The anodization time was controlled to produce 1.5 μm-thick AAO template on the initial Al layer. As-prepared AAO templates were directly dipped into 0.3M H_3PO_4 at 30 °C for 25 min for complete etching of the barrier oxide layer. The sequential processes for thinning and etching of the electrically resistive barrier oxide layer of AAO templates makes

the conductive Al layer exposed to electrolytes for subsequent Cu electrodeposition process. After washing the prepared AAO template with deionized water, artificial nuclei were prepared by electrodepositing tens nanometer-sized Ni nanoparticles at the bottom of the nanopores of AAO templates using Watt Bath, which has a well-optimized composition for controllable Ni electrodeposition [20]. Owing to the highly uniform dispersive artificial nucleation of Ni inside each pore, subsequent Cu electrodeposition was conformally achieved in the whole nanopores of AAO templates. After the removal of AAO templates with a mixture of 0.17 M phosphoric acid and 0.6 M chromic acid at 60 ^{o}C, well-ordered Cu nano-objects arrays on Al layers were obtained.

3.2 Cu electrodeposition inside nanopores of AAO templates without Ni artificial nuclei

Electrodeposition of Cu inside nanopores of AAO templates has been generally reported through a complicated procedure consisting of complete chemical etching of barrier oxide layer at the bottom of AAO templates and subsequent vacuum-deposition of conductive thin films on the as-opened pores [30, 31]. For Cu electrodeposition, we simplified the conventional procedure by removing the step for the conductive film vacuum-deposition, exploiting the remaining Al layer below the synthesized AAO template as an electrical contact for subsequent Cu electrodeposition. Unfortunately, the uniformly dispersive Cu nano-objects are hardly achieved with the prepared AAO templates. Figure 2 shows undesired severe overgrowth (Figure 2a) and seriously non-uniform nucleation of Cu at the bottom of nanopores (Figure 2b) in the initial stage of electrodeposition process, as illustrated in the inset schematic diagram. Unfortunately, this serious random electrodeposition behavior was observed even though intensive parameter optimization in the applied potential (Figure S2), the concentration of Cu^{2+} bath (Figure S3), barrier oxide layer etching time (Figure S4) and the duty cycle of the applied

pulse (Figure S5).

3.3 Preparation of artificial nuclei using Ni nanoparticle

Nucleation, which is the first step of electrodeposition, is the most important for achieving proper electrodeposition [32]. Obviously, uniform and stable nucleation over the whole surfaces of substrates is an essential prerequisite to achieve uniform nano-objects arrays using nanoporous template *via* electrodeposition process. Based on the failure of electrodeposition of Cu stemming from random nucleation at the bottom of nanopores, the artificial nucleation strategy was introduced by pre-electrodepositing of Ni, which has been well-known metal to allow controllable electrodeposition with well-optimized process condition. Evenly dispersed Ni nanoparticles of tens nanometer-diameter were uniformly formed inside the entire nanopores of AAO by pulse electrodeposition at -5.5 V vs. Ag/AgCl for 500 ms (100 cycles of a pulsed voltage), as shown Figure 3a, 3b and 3c. Contrary to the uncontrollable manner in the conventional electrodeposition of Cu, the pre-electrodeposited Ni artificial nuclei show highly uniform height and diameter without undesired Ni overgrowth on the top surface of AAO templates. The size of Ni artificial nuclei could be precisely controlled by adjusting the electrodeposition condition, as shown in Figure S6.

3.4 Highly uniform and controllable Cu electrodeposition inside nanopores *via* artificial nucleation with Ni nanoparticles

Figure 4 shows uniformly Cu filled nanopores of AAO templates. Electrodeposition of Cu was conducted with AAO template containing evenly formed Ni artificial nuclei at the bottom of the nanopores at -8.5 V vs. Ag/AgCl of a pulsed voltage for desired deposition time.

Surprisingly, the AAO with artificial nuclei allows stable and straightforward Cu electrodeposition inside the nanopores with high repeatability and reliability. Figure 4a shows a cross-sectional SEM image after Cu nano-object formation on Ni artificial nuclei. 300 nm-high Cu nanowires was successfully formed from Ni artificial nuclei with high uniformity without the uncontrolled overgrowth, frequently observed in Cu electrodeposition inside typical AAO templates. The high-magnified SEM observation in Figure 4b shows the electrodeposited Cu nano-objects and the underlying pre-electrodeposited Ni artificial nuclei with a distinguishable boundary due to heterogeneity between Cu and Ni. Interestingly, the unsolved challenge for large areal uniform formation of Cu nano-objects through electrodeposition technique were straightforwardly addressed by the artificial nucleation-assisted electrodeposition. Figure 4c and the inset image show a SEM image and a schematic diagram of highly uniformly formed Cu nano-objects produced by the artificial nucleation-assisted electrodeposition and subsequent AAO removal. The observed domain boundaries of Cu nano-objects arrays in the SEM image was exactly duplicated of the domain boundaries of the used AAO templates (Figure 4c and Figure S7). It strongly indicates that the novel electrodepositing strategy exploiting artificial nuclei enables a near perfect nano-templating for uniform fabrication of nano-objects with high uniformity. Figure 4d shows typical structures of Cu nano-objects arrays grown by the artificial nucleation-assisted electrodeposition. Figure 4e and f show Cu nano-object arrays produced by longer time electrodeposition. Owing to the relatively high aspect geometry, compared to those of Figure c and d, the produced longer Cu nano-object arrays were agglomerated after wet-etching of AAO template due to the capillary effect during drying process (Figure f), and eventually yield a work-like pattern (Figure e). The inset in Figure f shows a high magnified top-view SEM image of the agglomerated Cu nano-object arrays.

3.5. The effect of artificial Nucleation on Cu electrodeposition with AAO nanoporous templates

The effect of artificial nucleation on the Cu electrodeposition with AAO templates was investigated based on the relation between the reduction current and the electrodeposition time (I-t curve). Figure 5a shows overall I-t curve for whole sequential electrodeposition processes consisting of the formation of Ni nanoparticles as artificial nuclei and the growth of Cu nano-objects. After Ni pre-electrodeposition of 500 ms (100 pulse cycles), the electrolyte was changed to Cu^{2+} solution for followed Cu electrodeposition. The difference in the reduction current between Ni and Cu electrodeposition originates from the difference optimized electrodeposition condition each other in applied potential, electrolyte concentration and composition of electrolyte, as described in Experimental section.

Figure 5b shows a typical I-t curve for metal electrodeposition into a nanoporous template. In the I-t curve, there are four main stages: I) transient stage for metal nucleation; II) steady stage for metal growing in the pores; III) increasing stage when producing hemispherical metal caps start forming due to the rapid increase in the deposition area; IV) second steady stage for a planar and contiguous metallic top layer deposition after the coalescence of the caps [33]. Thus, nano-objects arrays obtained by filling the nanopores are generally formed by stopping the electrodeposition process at the transition point between region II and III. Figure 5c and 5d show y-axis magnified I-t curves of Ni and Cu electrodeposition in Figure 5a, respectively. According to the typical I-t curve model for metal electrodeposition inside nanoporous templates, those two I-t curves clearly show Stage I and II mentioned in Figure 5b during Ni and Cu electrodeposition, indicating uniform and stable metal electrodeposition inside

nanopores of the template. Eventually, the Ni artificial nuclei effectively induced controllable growth of Cu nano-objects in the nanoporous template. In contrast, Cu electrodeposition using AAO template without Ni artificial nuclei showed the rapid increase in the reduction current from the early stage of Cu electrodeposition during a short time of initial 20 ms (4 pulse cycles), and maintained the current value for a desired time. It implies a seriously non-uniform nucleation among nanopores of AAO templates (Figure S8). It leads to a rapid transition from Stage II to Stage III and IV in a few electrochemically activated nanopores, causing random growth of Cu nano-objects (inset image of Figure 5e). The brilliant strategy using the artificial nucleus for electrochemical deposition into nanoporous template effectively addresses the issues of unexpected random nucleation and the resulting overgrowth.

3.6. Precise control of the height of Cu nano-objects

Uniform and stable electrodepositing behavior based on the artificial nucleation offers a precise controllability in the structure of nano-objects produced by electrodeposition. Figure 6a-f show cross-sectional SEM images of the Cu nano-objects of various height in AAO templates. The height of each Cu nano-objects was precisely controlled by adjusting an electrodeposition time of 125(25), 250(50), 500(100), 1000(200) 2000(400) and 3500 ms (700 pulse cycles), respectively. As shown in Figure 6g, the growth rate of Cu nano-objects was calculated to 3.49 nm per each pulse cycle, which is linearly proportional to the electrodeposition time (the number of pulse cycle) up to 2000 ms (400 pulse cycles). After the formation of the hemispherical caps on the top surface of AAO templates at the 2000 ms (400 pulse cycles) as shown in Figure 6e, the planar electrodeposition of Cu was observed at the 3500 ms (700 pulse cycles) as shown in Figure 6g. Accordingly, the estimated Cu electrodeposition rate in this planar deposition region was changed to 0.27 nm per each pulse cycle.

3.6. Precise control of the diameter of Cu nano-objects

The diameter of the electrochemically grown Cu nano-objects is determined by the pore size of AAO templates. The pore size of AAO template is highly dependent on the anodization condition including pH of electrolyte, the magnitude of applied voltage and pore widening time [34]. In this work, pH of electrolyte and corresponding applied voltage was selectively adjusted for the precise control of the size of nanopores in the range from a few nanometers to tens nanometers (Figure 7a and Figure S9). Figure 7b shows top-view SEM images of pore size-controlled AAO templates. Using the pore-sized controlled AAO for artificial nucleation-assisted electrodeposition, Cu nano-objects with various diameters were successfully synthesized as show in Figure c-f.

4. Conclusions

In summary, we have demonstrated a straightforward, reliable and controllable electrochemical route to Cu nano-objects *via* novel artificial nucleation-assisted electrodeposition using nanoporous AAO template. The pre-electrodeposited Ni nanoparticle at the bottom of the AAO templates effectively plays a role as a nucleus for the stable and uniform Cu electrodeposition inside the nanopores. The artificial nucleation reliably addresses the severe non-uniform overgrowth of Cu of typical AAO templates by offering effective nucleus for further growth of Cu at the early stage of electrodeposition process. Based on the highly uniform electrodepositing behavior by introducing the artificial nuclei, the geometry of Cu nano-objects can be precisely controlled by manipulating electrodeposition time and the pore diameter of AAO templates. This highly reproducible and facile electrodeposition principle exploiting

artificial nuclei inside nanoporous template will greatly broaden the potential of electrochemical synthesis of nano-objects for electronics, energy devices and environmental applications.

Appendix A. Supplementary data

Supplementary data to this article can be found online at

Author Contributions

Joonwon Lim: Conceptualization, Methodology, Investigation, Writing-Original draft preparation, Writing-Review & Editing, Visualization. Ki-Hwan Kim: Methodology, Investigation. Costel-Sorin Cojocaru: Supervision.

Acknowledgements

This work was supported by the National Research Foundation of Korea (NRF) grant funded by the Korean government (MSIT) (No.2021R1F1A1061182).

References

[1] Z. Yang, J. Zhang, M.C. Kintner-Meyer, X. Lu, D. Choi, J.P. Lemmon, J. Liu, Electrochemical energy storage for green grid, Chem. Rev. 111(5) (2011) 3577-3613.

[2] Y.G. Guo, J.S. Hu, L.J. Wan, Nanostructured materials for electrochemical energy conversion and storage devices, Adv. Mater. 20(15) (2008) 2878-2887.

[3] C.R. Martin, Membrane-based synthesis of nanomaterials, Chem. Mater. 8(8) (1996) 1739-1746.

[4] J. Lim, U.N. Maiti, N.-Y. Kim, R. Narayan, W.J. Lee, D.S. Choi, Y. Oh, J.M. Lee, G.Y. Lee, S.H. Kang, Dopant-specific unzipping of carbon nanotubes for intact crystalline graphene nanostructures, Nat. Commun. 7(1) (2016) 1-9.

[5] J. Lim, J.-W. Jung, N.-Y. Kim, G.Y. Lee, H.J. Lee, Y. Lee, D.S. Choi, K.R. Yoon, Y.-H. Kim,

I.-D. Kim, N2-dopant of graphene with electrochemically switchable bifunctional ORR/OER catalysis for Zn-air battery, Energy Storage Mater. 32 (2020) 517-524.

[6] G.H.A. Therese, P.V. Kamath, Electrochemical synthesis of metal oxides and hydroxides, Chem. Mater. 12(5) (2000) 1195-1204.

[7] R. Xiao, S.I. Cho, R. Liu, S.B. Lee, Controlled electrochemical synthesis of conductive polymer nanotube structures, J. Am. Chem. Soc. 129(14) (2007) 4483-4489.

[8] R.M. Penner, Mesoscopic metal particles and wires by electrodeposition, J. Phys. Chem. B 106(13) (2002) 3339-3353.

[9] X. Ma, Z. Liu, H. Chen, Facile and scalable electrodeposition of copper current collectors for high-performance Li-metal batteries, Nano Energy 59 (2019) 500-507.

[10] K. Edström, D. Brandell, T. Gustafsson, L. Nyholm, Electrodeposition as a tool for 3D microbattery fabrication, Electrochem. Soc. Interface 20(2) (2011) 41.

[11] E.C. Walter, M.P. Zach, F. Favier, B.J. Murray, K. Inazu, J.C. Hemminger, R.M. Penner, Metal nanowire arrays by electrodeposition, ChemPhysChem 4(2) (2003) 131-138.

[12] M.P. Zach, K.H. Ng, R.M. Penner, Molybdenum nanowires by electrodeposition, Science 290(5499) (2000) 2120-2123.

[13] X. Li, J. Mo, J. Fang, D. Xu, C. Yang, M. Zhang, H. Li, X. Xie, N. Hu, F. Liu, Vertical nanowire array-based biosensors: device design strategies and biomedical applications, J. Mater. Chem. B 8(34) (2020) 7609-7632.

[14] A. Yin, J. Li, W. Jian, A. Bennett, J. Xu, Fabrication of highly ordered metallic nanowire arrays by electrodeposition, Appl. Phys. Lett. 79(7) (2001) 1039-1041.

[15] J. Martín, M. Martín-González, J.F. Fernández, O. Caballero-Calero, Ordered three-dimensional interconnected nanoarchitectures in anodic porous alumina, Nat. Commun. 5(1) (2014) 1-9.

[16] Y. Yamamoto, N. Baba, S. Tajima, Coloured materials and photoluminescence centres in

anodic film on aluminium, Nature 289(5798) (1981) 572-574.

[17] C.-W. Tao, T.-J. Yen, T.-Y. Huang, Achieving sub-wavelength imaging through a flat hyperlens in a modified anodic aluminum oxide template, Sci. Rep. 10(1) (2020) 1-7.

[18] K.H. Kim, D. Brunel, A. Gohier, L. Sacco, M. Châtelet, C.S. Cojocaru, Cup-Stacked Carbon Nanotube Schottky Diodes for Photovoltaics and Photodetectors, Adv. Mater. 26(25) (2014) 4363-4369.

[19] J. Liu, F. Wang, J. Zhai, J. Ji, Controllable growth and magnetic characterization of electrodeposited nanocrystalline Ni–P alloy nanotube and nanowire arrays inside AAO template, J. Electroanal. Chem. 642(2) (2010) 103-108.

[20] K. Nielsch, F. Müller, A.P. Li, U. Gösele, Uniform nickel deposition into ordered alumina pores by pulsed electrodeposition, Adv. Mater. 12(8) (2000) 582-586.

[21] W. Lee, K. Schwirn, M. Steinhart, E. Pippel, R. Scholz, U. Gösele, Structural engineering of nanoporous anodic aluminium oxide by pulse anodization of aluminium, Nat. Nanotech. 3(4) (2008) 234-239.

[22] L. Wen, R. Xu, Y. Mi, Y. Lei, Multiple nanostructures based on anodized aluminium oxide templates, Nat. Nanotech. 12(3) (2017) 244-250.

[23] O. Jessensky, F. Müller, U. Gösele, Self-organized formation of hexagonal pore arrays in anodic alumina, Appl. Phys. Lett. 72(10) (1998) 1173-1175.

[24] B. Marquardt, L. Eude, M. Gowtham, G. Cho, H.J. Jeong, M. Châtelet, C.S. Cojocaru, B. Kim, D. Pribat, Density control of electrodeposited Ni nanoparticles/nanowires inside porous anodic alumina templates by an exponential anodization voltage decrease, Nanotechnology 19(40) (2008) 405607.

[25] T. Moffat, D. Wheeler, W. Huber, D. Josell, Superconformal electrodeposition of copper, Electrochem. Solid-State Lett. 4(4) (2001) C26.

[26] T.P. Moffat, J. Bonevich, W. Huber, A. Stanishevsky, D. Kelly, G. Stafford, D. Josell,

Superconformal electrodeposition of copper in 500–90 nm features, J. Electrochem. Soc. 147(12) (2000) 4524.

[27] S. Wang, Y. Tian, C. Wang, C. Hang, H. Zhang, Y. Huang, Z. Zheng, One-step fabrication of copper nanopillar array-filled AAO films by pulse electrodeposition for anisotropic thermal conductive interconnectors, ACS Omega 4(4) (2019) 6092-6096.

[28] F. Jiang, L. Qi, G. Song, H.-Z. Yu, Carbon tape-assisted electrodeposition and characterization of arrayed micro-/nanostructures, Electrochim. Acta 380 (2021) 138192.

[29] Y. Konishi, M. Motoyama, H. Matsushima, Y. Fukunaka, R. Ishii, Y. Ito, Electrodeposition of Cu nanowire arrays with a template, J. Electroanal. Chem. 559 (2003) 149-153.

[30] G.D. Sulka, A. Brzózka, L. Liu, Fabrication of diameter-modulated and ultrathin porous nanowires in anodic aluminum oxide templates, Electrochim. Acta 56(14) (2011) 4972-4979.

[31] C. Tran, J. Santos-Peña, C. Damas, Electrodeposited manganese oxide supercapacitor microelectrodes with enhanced performance in neutral aqueous electrolyte, Electrochim. Acta 335 (2020) 135564.

[32] Y. Feng, K.-D. Kim, C.A. Nemitz, P. Kim, T. Pfadler, M. Gerigk, S. Polarz, J.A. Dorman, J. Weickert, L. Schmidt-Mende, Uniform large-area free-standing silver nanowire arrays on transparent conducting substrates, J. Electrochem. Soc. 163(8) (2016) D447.

[33] T. Whitney, P. Searson, J. Jiang, C. Chien, Fabrication and magnetic properties of arrays of metallic nanowires, Science 261(5126) (1993) 1316-1319.

[34] A. Belwalkar, E. Grasing, W. Van Geertruyden, Z. Huang, W. Misiolek, Effect of processing parameters on pore structure and thickness of anodic aluminum oxide (AAO) tubular membranes, J. Membr. Sci. 319(1-2) (2008) 192-198.

Figure Legends

Figure 1. Synthetic procedure for Cu nano-objects based on artificial nucleation-assisted electrodeposition using nanoporous AAO templates.

Figure 2. Typical failure of uniform electrodeposition of Cu with nanoporous AAO templates. (a) Non-uniform overgrowth of Cu on the top surface of AAO templates. (b) Random nucleation of Cu at the bottom of nanopores of AAO template at the early stage of electrodeposition process.

Figure 3. The uniform formation of artificial nuclei at the bottom of the nanopores of AAO template. (a-c) Cross-sectional SEM images of uniformly electrodeposited Ni nanoparticles used as artificial nuclei for following Cu electrodeposition. (d) Top-view SEM image of Ni nanoparticles formed at the bottom of the nanopores after removal of AAO templates.

Figure 4. Highly uniform Cu nano-objects arrays synthesized by the artificial nucleation-assisted electrodeposition. (a) Cross-sectional SEM images of Cu nano-objects arrays on the Ni artificial nuclei inside AAO template. (b) Magnified SEM images of Cu nano-objects on the underlying Ni nanoparticles. (c, d) Highly uniform Cu nano-objects arrays of 700 nm-height after removal of AAO template. (e, f) Highly uniform Cu nano-objects arrays of 1500 nm-height after removal of AAO template.

Figure 5. I-t curve for artificial nucleation-assisted electrodeposition of Cu. (a) I-t curve for

the artificial nucleation-assisted electrodeposition consisting of sequential formation of Ni and Cu inside the nanopores of AAO template. (b) Typical I-t curve for metal electrodeposition using nanoporous AAO template. (c) I-t curve for Ni pre-electrodeposition for artificial nuclei preparation. (d) I-t curve for Cu electrodeposition for nano-objects growth inside AAO template. (e) I-t curve for non-uniform growth of Cu nano-objects without artificial nuclei at the bottom of the nanopores.

Figure 6. Precise control of the height of Cu nano-objects by adjusting the electrodeposition time (the number of pulse cycle). (a-f) Cross-sectional SEM images of Cu nano-objects with underlying Ni artificial nuclei electrodeposited with various cycle number of pulsed voltage of -8.5 V (with working regime 5 ms and resting regime of 95 ms) vs. Ag/AgCl of 25, 50, 100, 200, 400 and 700 cycles, respectively. Each cycle number correspond to the electrodepositing time duration of 125, 250, 500, 1000, 2000 and 3500 ms, respectively. (g) The plot of the number of pulse cycle vs. the height of grown Cu nano-objects.

Figure 7. Precise control of the diameter of Cu nano-objects by manipulating the pore size of AAO templates. (a) The change of the pore size of AAO template under the various anodization and pore widening conditions. (b) Top-view SEM images of As-prepared AAO templates with various pore diameters. (c-f) Top-view SEM images of electrodeposited Cu nano-objects with various diameters.

Figure 1.

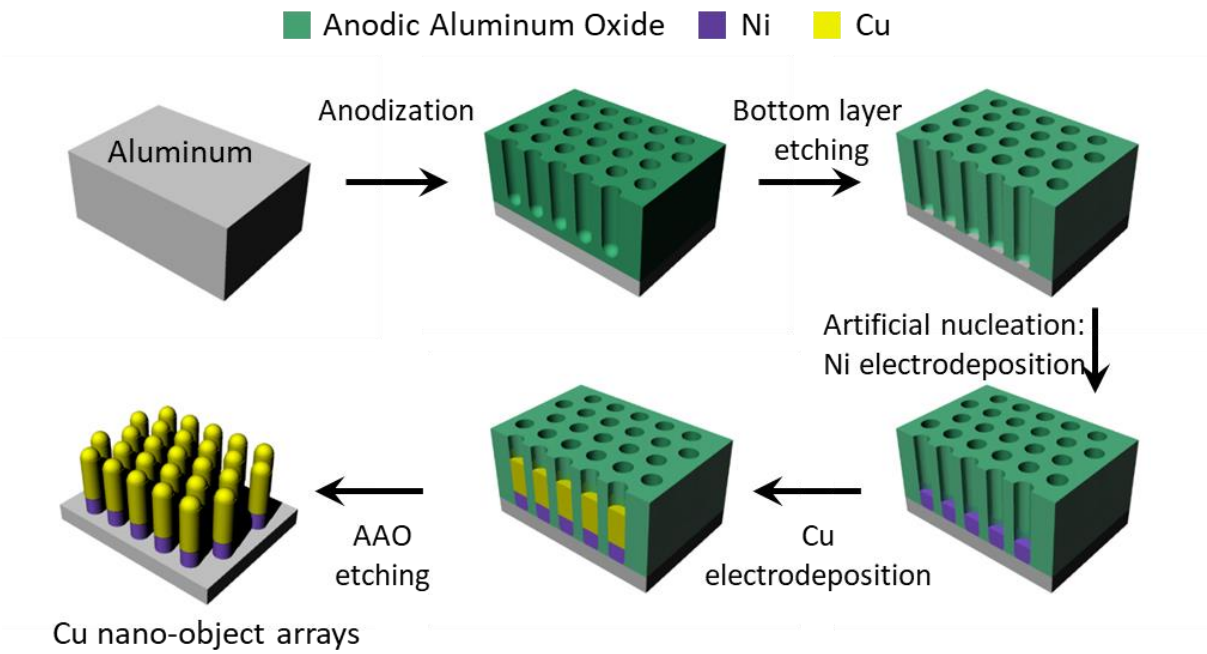
Anodic Aluminum Oxide
Ni
Cu
Aluminum
Anodization
Bottom layer etching
Artificial nucleation: Ni electrodeposition
Cu electrodeposition
AAO etching
Cu nano-object arrays

Figure 2.

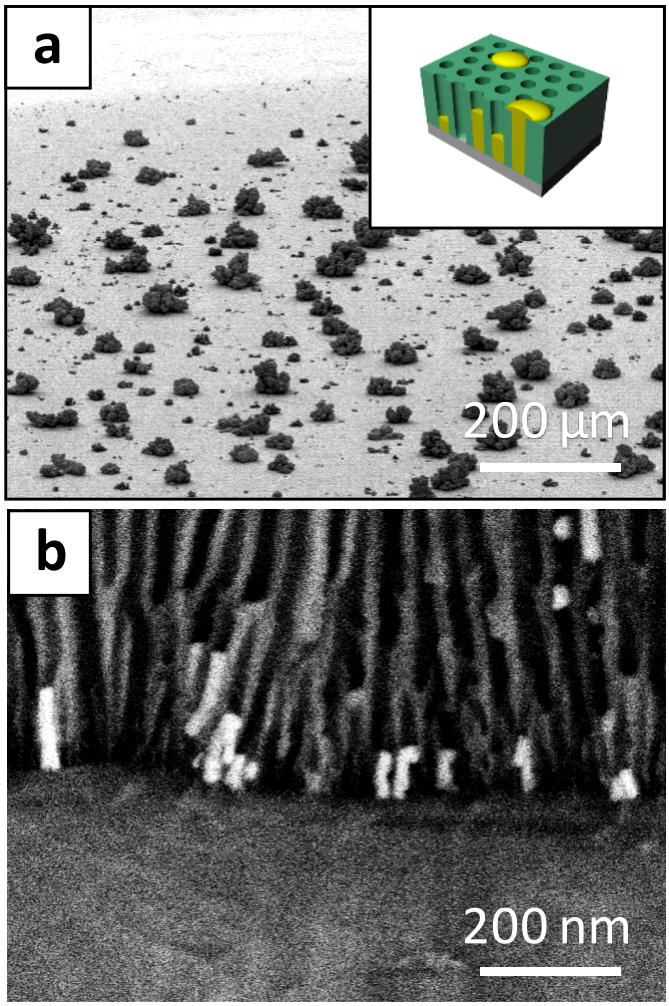

Figure 3.

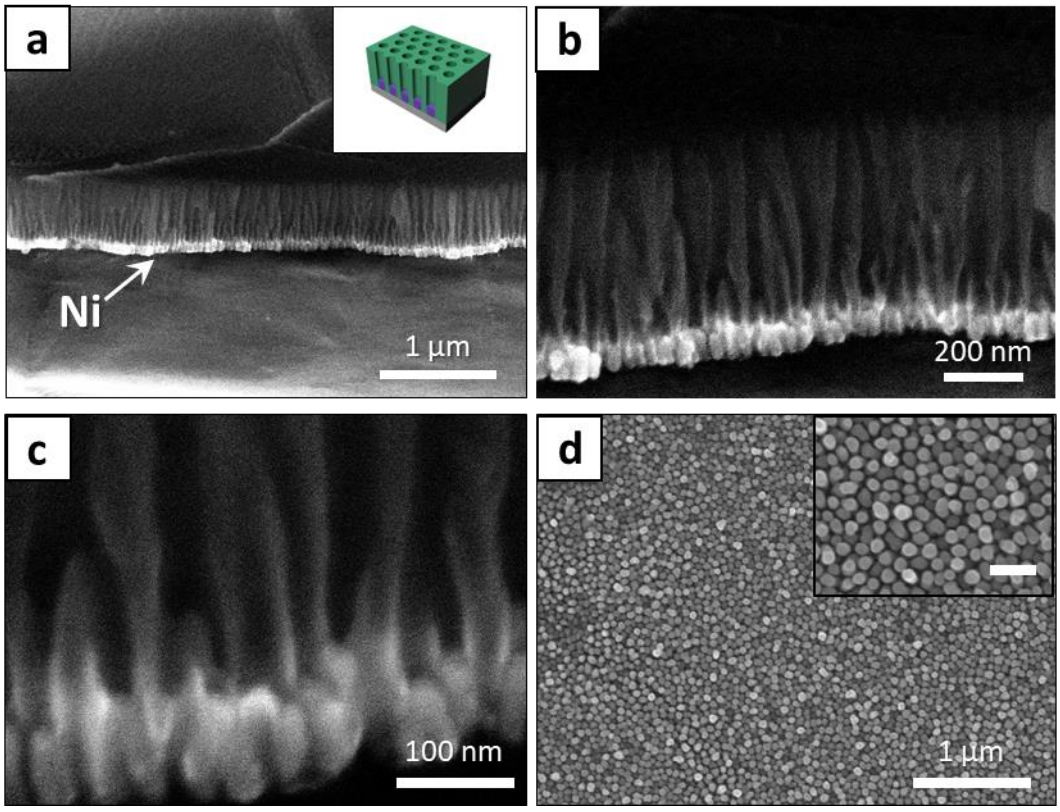

Figure 4.

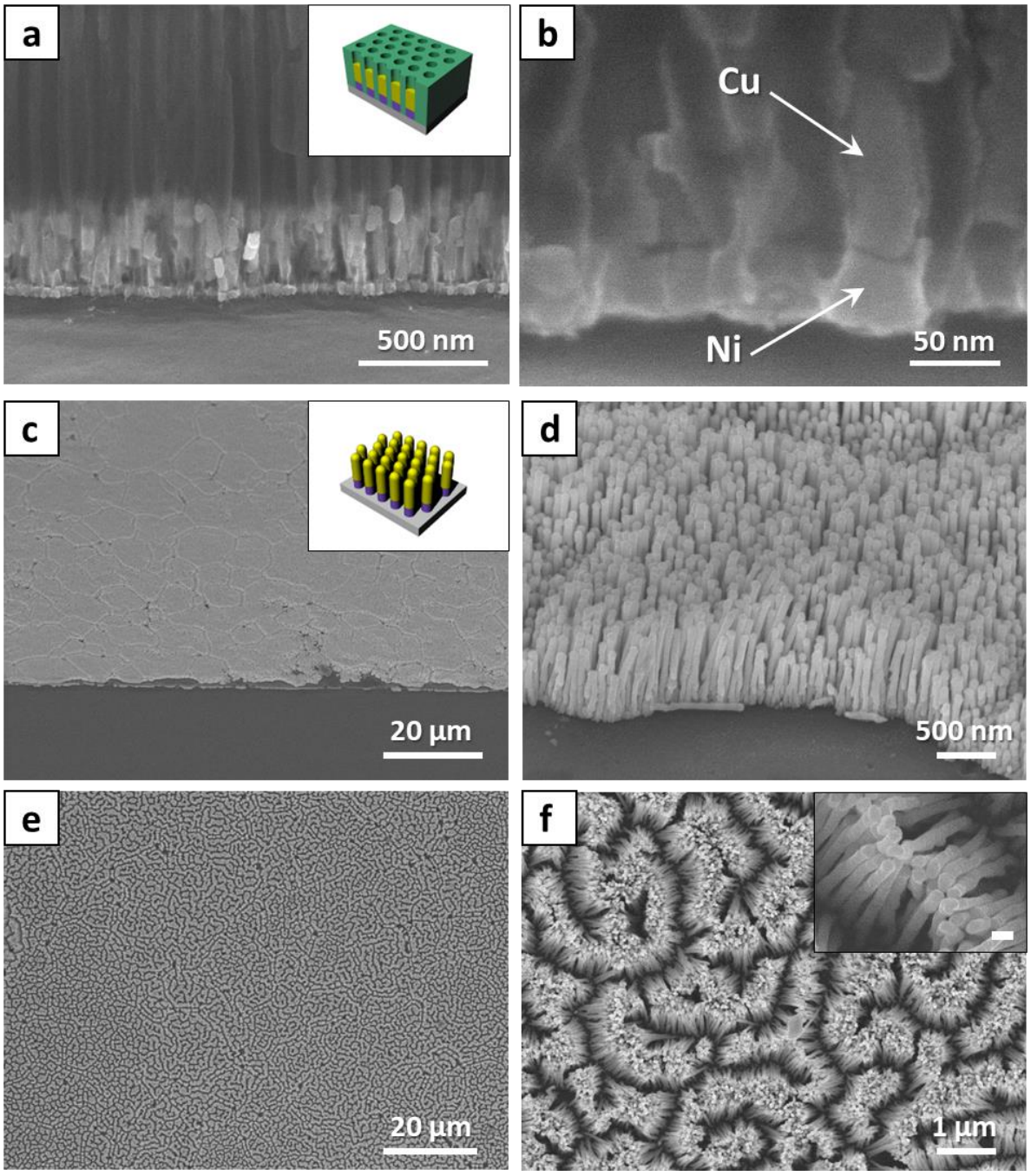

Figure 5.

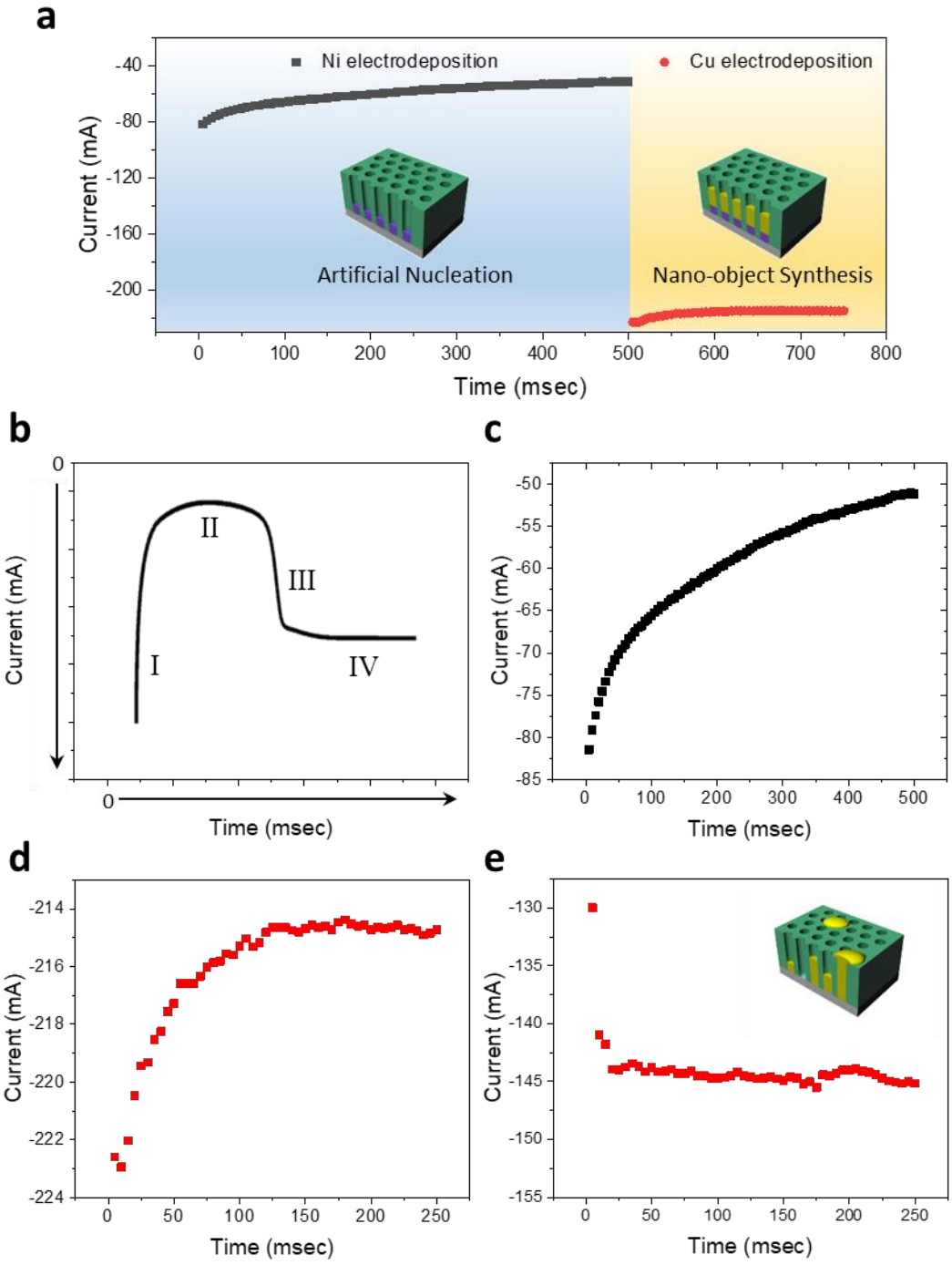
a
Ni electrodeposition
Cu electrodeposition
Artificial Nucleation
Nano-object Synthesis
Current (mA)
Time (msec)
b
I
II
III
IV
Current (mA)
Time (msec)
c
Current (mA)
Time (msec)
d
Current (mA)
Time (msec)
e
Current (mA)
Time (msec)

Figure 6.

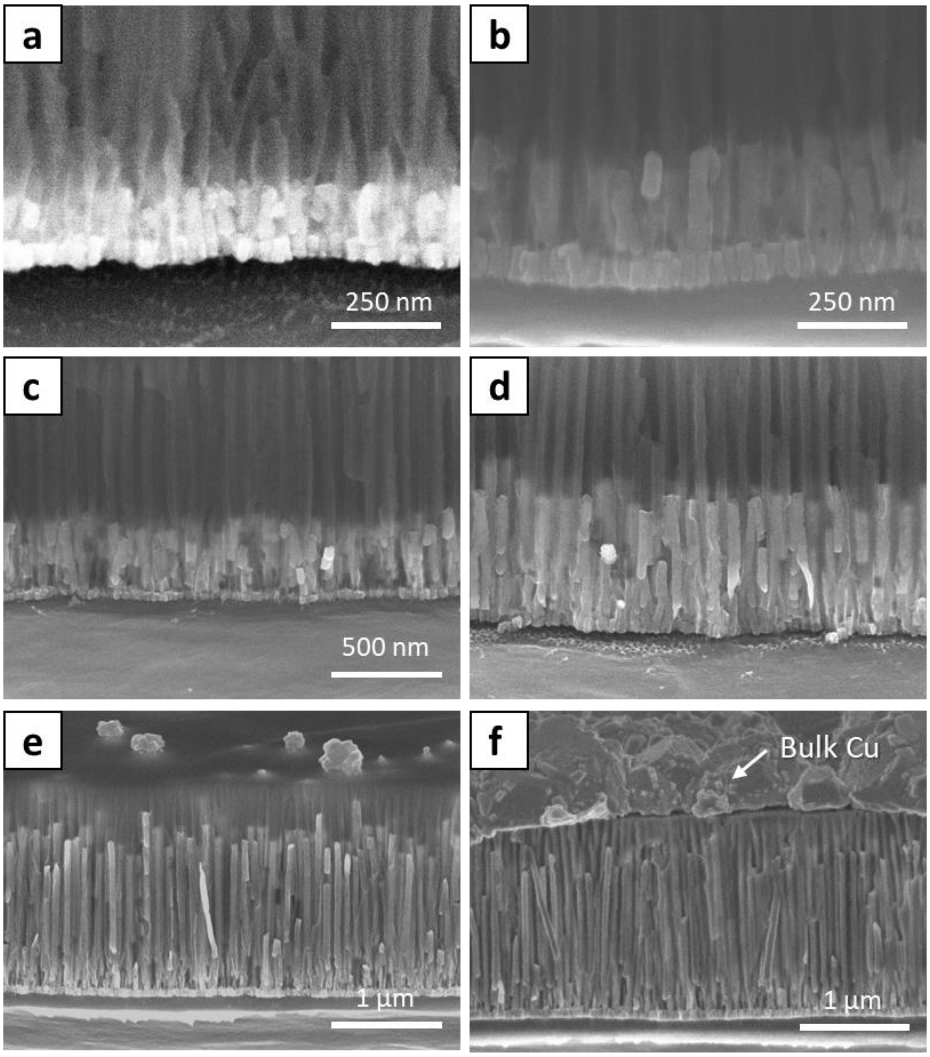
a
250 nm
b
250 nm
c
500 nm
d
e
1 µm
f
Bulk Cu
1 µm

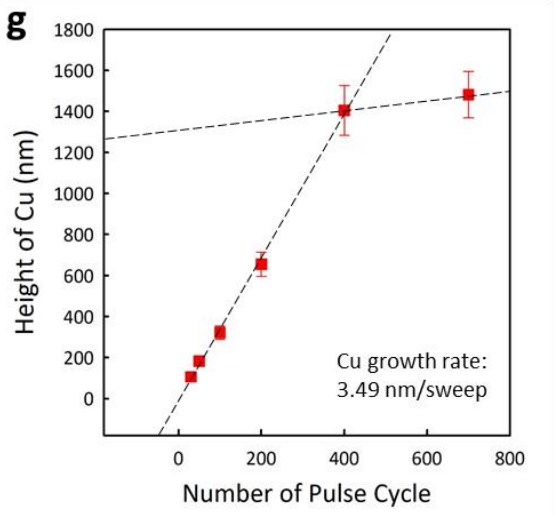
g
Height of Cu (nm)
1800
1600
1400
1200
1000
800
600
400
200
0
0
200
400
600
800
Number of Pulse Cycle
Cu growth rate:
3.49 nm/sweep

Figure 7

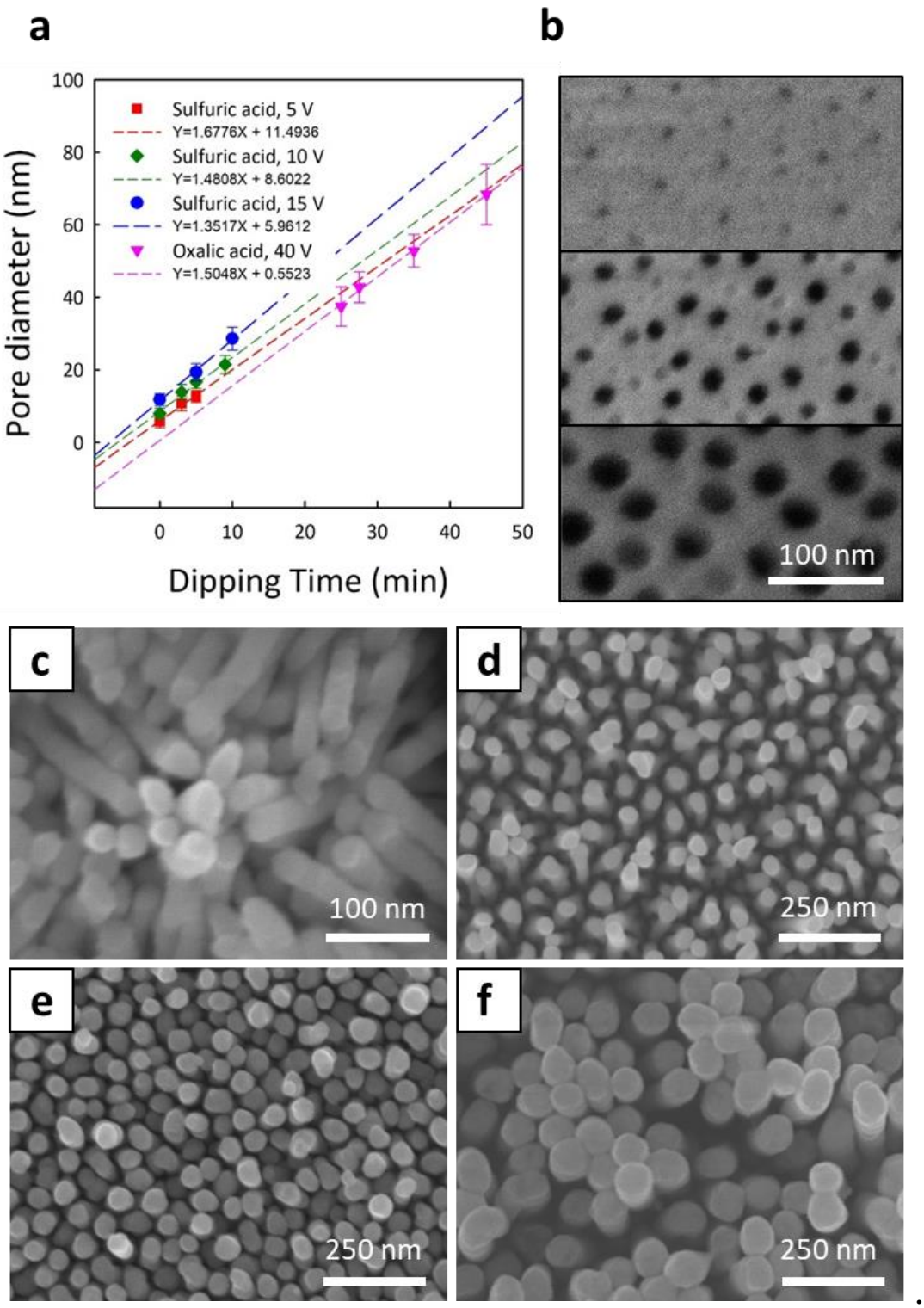
a
b
Pore diameter (nm)
Dipping Time (min)
Sulfuric acid, 5 V
Y=1.6776X + 11.4936
Sulfuric acid, 10 V
Y=1.4808X + 8.6022
Sulfuric acid, 15 V
Y=1.3517X + 5.9612
Oxalic acid, 40 V
Y=1.5048X + 0.5523
100 nm
c
100 nm
d
250 nm
e
250 nm
f
250 nm